ACS APPLIED ENERGY MATERIALS

www.acsaem.org

Article

Optimized Interfaces for PBI-Based High-Temperature Direct Ethanol Fuel Cells

Rodrigo Pires da Silva, Bruno Ribeiro de Matos,* Fabio Coral Fonseca, and Elisabete Inacio Santiago

Cite This: ACS Appl. Energy Mater. 2024, 7, 7759−7768

Read Online

ACCESS | Metrics & More | Article Recommendations | Supporting Information

ABSTRACT: The present study combines innovative strategies aiming at enhanced performance of direct ethanol fuel cells (DEFC) by modifying interfaces at both electrodes and electrolyte. Increasing the operating temperature to 180 °C to promote faster kinetics and thermally activated processes taking place in DEFC was possible by using phosphoric-acid-doped PBI (polybenzimidazole) composite electrolytes. The properties of the PBI electrolytes were improved by adding SiO_2 as an inorganic second phase, promoting an increase in the proton conductivity and inhibiting ethanol crossover. Optimizing electrode reactions by increasing the triple-phase boundary was demonstrated by using a powdered-based PBI "ionomeric" concept to boost the performance of the proton exchange membrane fuel cell. The electrochemical characterization of the high-temperature direct ethanol fuel cells (HT-DEFC) showed that combining the strategies for the optimized electrode and electrolyte was crucial for increasing the performance of membrane electrode assemblies operating at 180 °C.

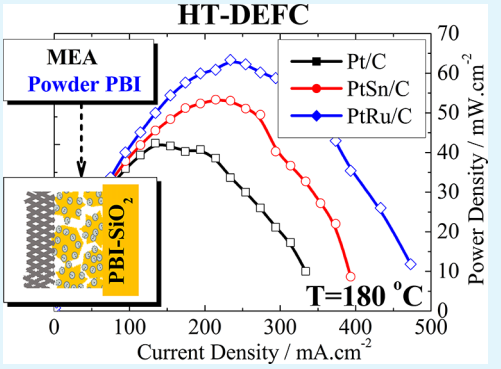

KEYWORDS: *direct ethanol fuel cell, polybenzimidazole, composite membranes, binder, triple-phase boundary, interfaces*

1. INTRODUCTION

Direct ethanol fuel cells (DEFC) are regarded as a promising technology to confront the alarming environmental challenges denounced in the latest IPCC report.[1] The major advantage of DEFC relies on its deployment simplicity compared to other fuel cell systems that require large infrastructure investments.[2] This is the scenario in several countries where the infrastructure for green ethanol utilization has already been implemented, such as Brazil, China, the EUA, and India. On the other hand, the application of hydrogen-fed fuel cells has numerous hurdles associated with production, storage, distribution, maintenance, and the development of the technology itself.[2]

Meanwhile, the commercialization of DEFC depends solely on a necessary and challenging breakthrough: the DEFC components development to overcome its main and problematic deficiency, namely, the low empirical efficiency (12−30%)[3] compared to its outstanding theoretical efficiency of 96%. The reasons for such low efficiency are the sluggish kinetics of ethanol oxidation and the elevated ethanol crossover through the electrolyte, which aggravates the cathodic oxygen reduction reaction, preventing it from harnessing the available 12 electrons contained in the acid acetic and acetaldehyde as the main reaction subproducts. One of the timely alternatives for boosting DEFC efficiency is the rise of the operating temperature departing from the current 80 °C. Since the electrode and ionic processes are thermally activated, the increase of the operating temperature can boost the DEFC performance. However, to achieve efficient operation at high temperatures, it is necessary to replace the state-of-the-art Nafion with a thermally stable electrolyte. Such limitation can be overcome by using a high-performance engineering electrolyte from the polyimide family, termed polybenzimidazole (PBI).

The performance of the DEFC electrode and electrolyte components can be enhanced with the use of PBI membranes, which can promisingly increase the operating temperature range from 100 °C up to 200 °C.[4,5] PBI has excellent chemical stability and mechanical resistance at elevated temperatures with a glass transition occurring in the range of 450 to 500 °C, mainly a result of its rigid backbone composed of heteroaromatic ring structure;[9] most conventional polymers have a glass transition ranging from −130 to 150 °C. Despite being hygroscopic, at high temperatures, it absorbs a small amount of water, which facilitates the DEFC operation at low relative humidity, thereby decreasing the amount of ethanol dissolved in water and its crossover. When doped with phosphoric acid, PBI reaches high values of conductivity at high temperatures.[9] All of these factors are considered crucial

Received: May 13, 2024
Revised: August 17, 2024
Accepted: August 26, 2024
Published: September 2, 2024

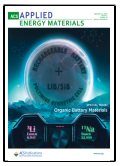

aspects to improve the performance of the DEFC at high temperatures.

The further improvement of PBI by the addition of a second inorganic phase was previously pursued. The reduction of the ethanol crossover can be attained by composite electrolytes; the presence of dispersed nanoparticles in the polymer decreases the mean free path for the diffusion of ethanol and oxidized subproducts and therefore diminishes the rate of cathode poisoning.[6−8] Numerous previous results confirm the alcohol crossover reduction in the composite membrane.[10−20] Several types of nanoparticles, varying in shape, composition, and functionalization, have been inserted in PBI aiming at improved properties such as silicon dioxide (SiO_2),[10−13] titanium dioxide (TiO_2),[14,15] zirconium dioxide (ZrO_2),[18,19] and phosphotungstic acid ($H_4Si(W_3O_{10})_4$).[16,17]

The addition of mesoporous and surface-functionalized silica into PBI containing sorbed ionic liquids 1,3-di(3-methylimidazolium) has shown to display a high proton conductivity (0.22 $S{\cdot}cm^{-1}$) even at anhydrous condition.[10] Another study investigated the use of silica nanofibers functionalized with acidic ($-SO_3H$) and basic ($-NH_2$) groups into a PBI matrix. A high proton conductivity was achieved at 200 °C (4 $mS{\cdot}cm^{-1}$) considering that the PBI was not imbibed with phosphoric acid.[12] The addition of solid acids in conjunction with mesoporous silica nanoparticles into the PBI matrix, such as $KH_5(PO_4)_2$, resulted in an enhancement of the mechanical strength at 180 °C.[13] The composite membranes possibly exhibited the superprotonic conductivity transition due to the solid acid producing as an outcome an enhanced fuel cell performance (36 $mW{\cdot}cm^{-2}$) compared to the pristine membrane (10 $mW{\cdot}cm^{-2}$).[13] Likewise, the utilization of PBI-SiO_2 composites promoted significant improvement in fuel cells fed with alcohols.[20] The PBI-SiO_2 composites doped with phosphoric acid displayed suppression of the methanol crossover in DMFC (direct methanol fuel cell) at 200 °C. It is proposed that the formation of phosphosilicates inhibits the alcohol transport through the membrane resulting in a high fuel cell performance at high temperature.[20] In general, the inorganic phase has functional hydroxyl groups attached at the surface, which modifies the dynamics of the segmental motion of the PBI chains via acid−base interactions as revealed by broadband dielectric spectroscopy.[9,21] These intimate interactions among organic and inorganic phases synergistically enhance the proton conduction properties of the polymer at high temperatures.[22,23] Moreover, the PBI composites are shown to be able to increase the phosphoric acid retention due to the interactions of organic and inorganic salts with the polymer phase.[22,23]

Regarding relevant aspects for electrode optimization in HT fuel cells, the ionomeric phase, which supplies the ion-conducting phase in the triple-phase boundary, has been pointed out as a crucial component in both fuel cell performance and durability. Specifically, for PBI-based fuel cells, it has been discussed what would be the proper binder selection that improves the catalytic activity at high operating temperatures.[24,25] Hydrophobic electrode binders such as PTFE, PVDF, and polyurethane have been preferred over PBI binder since the hydrophobic moieties of these polymers promote an increase of the electrochemically active surface area (ECSA), thereby boosting the fuel cell performance at low and high current densities, mostly associated with the catalytic activity and mass transport within the electrodes, respectively.[24,25] However, a gradual study covering an interplay between hydrophilic and hydrophobic parts of polymeric binders was performed for phosphonated PTFE.[25] As a main outcome, the highest peak power densities evaluated over successive cycles for phosphonated PTFE showed better durability over PTFE,[25] which was assigned to a combination of both hydrophobic and proton conducting properties of the phosphonated binder.[25] It is worth noting that a binder bestowed with proton conducting properties is very promising for DEFC since the proton conductivity in alcoholic media is dramatically reduced.[26] Moreover, the use of PBI as a binder can even improve the proton conductivity due to a low contact resistance with the PBI electrolyte.[24]

Recent advances in the understanding of the triple-phase boundary have evidenced that higher fuel cell performance was obtained with the electrodes containing the ionomer in the powder form for anion exchange membrane fuel cells (AEMFC).[27,28] The use of poly(ethylene-*co*-tetrafluoroethylene) in the powder form (<100 μm) at the catalytic layer in an AEMFC fed with H_2/O_2 at 50 °C resulted in an increase of the peak power density from ∼180 to 240 mW cm^{-2}.[27] The electrochemical characterization indicated that an improved extension of the triple-phase boundary is reached by using the ionomer in the powdered form.[27,28]

Matching the morphologies of the electron and ionic conducting phases is critically important for reaching a high fuel cell performance. Traditionally, the catalyst layer of most ion exchange membrane fuel cells is made of a mixture of the catalyst and an ionomer binder (mostly benchmark Nafion dispersions) in an alcohol solution.[29] As a dispersion, Nafion consists of perfluorinated acid aggregates in the nanometric order, and when such dispersion is evaporated in the gas diffusion electrodes, it renders a thin Nafion film covering the electrocatalysts.[29] Such results suggest that a similar investigation for PBI materials is a promising and original strategy. The importance of such development for HT-DEFC is immediate since it necessitates both an alternative "ionomeric" phase and an improved triple-phase boundary for high-temperature operation, which are not achieved by Nafion-based ionomer in HT-PEMFC.

Most of the reported advances in fuel cell performance address a target component solely and separately, the catalyst/support, the catalyst binder, or even the electrolyte material. This one-by-one methodology is applied for the study of the performances of membrane electrode assembly (MEA) among many scientific reported data and is shown to render stepwise improvements compared to a benchmark reference data, which impairs further fuel cell advances by assessing the core electrochemical processes taking place at those interfaces. Thus, a systematic investigation of the synergistic effects at HT-PEMFC and HT-DEFC using PBI-based interfaces can provide valuable insights.

Herein, the enhancement of the DEFC efficiency was achieved by modifying key interfaces that contribute to the performance of electrochemical processes taking place at both the electrodes and the electrolyte. The main driver is increasing the operating temperature of the device, which requires adequate materials and interfaces. The main strategies tested were: (i) the use of high-temperature-resistant non-fluorinated PBI polymer at both electrode and electrolyte that allows increasing the operating temperature to 180 °C; (ii) the replacement of the solution cast catalyst layer to a PBI "ionomeric" phase in the powder form and using an electrocatalyst tailored for ethanol; and (iii) increasing

https://doi.org/10.1021/acsaem.4c01232
ACS Appl. Energy Mater. 2024, 7, 7759−7768

conductivity and thermal stability of the PBI electrolyte by the addition of silica nanoparticles. To obtain reliable results, the fuel cell components (electrode and electrolyte compositions) were optimized for hydrogen operation prior to the DEFC tests. The optimized configuration of the electrode and electrolyte resulted in high-performance DEFC at 180 °C. And the difficulty encountered in the analysis of electrode/electrolyte contributions due to the non-ohmic properties in the ion conduction of PBI is briefly discussed.

2. EXPERIMENTAL SECTION

2.1. Membrane Preparation. For the preparation of the reference PBI membrane, the PBI powder (Celazone, PBI Performance Products, Inc.) was solubilized in dimethylacetamine (DMA, Sigma-Aldrich) in the respective DMA/PBI mass ratio of 50:1. Lithium chloride (LiCl, Sigma-Aldrich) was employed as a stabilizing agent in a PBI/LiCl mass ratio of 18:1. The LiCl prevents the chain aggregation through −NH− and −NH═ interactions by $Li^+ - NH═$ and Cl^-−NH− stabilization, leading to a homogeneous solution. These materials were placed in a Teflon-lined autoclave, which was subsequently placed in a stirred oil bath at 200 °C for 6 h. The following step consisted of filtering the resulting solution to eliminate the undissolved PBI, thereby obtaining the characteristic limpid and brownish PBI solution. Thus, the PBI/DMA solution was transferred to a Petri dish, and membranes with 40 μm were produced by casting in a resistive furnace at 120 °C for 360 min at a heating rate of 20 °C·min^{-1}. The same procedure was used for the preparation of the composite membrane PBI-SiO_2. In an additional step to the preparation of PBI-SiO_2 composite membranes, silica powder (Aldrich, particle size 5−15 nm) was added to the PBI/DMA solution, and the resulting mixture was placed in an ultrasonic stirrer for 2 min to homogenize the distribution of the nanoparticles. The final PBI-SiO_2/DMA mixture becomes transparent upon stirring, which indicates that such a procedure was essential to disrupting large silica particle aggregates. The PBI-SiO_2 composite membranes were prepared with 2.5, 5, and 10 wt % of silica. All of the prepared membranes were submitted to cleaning baths in H_2SO_4 (0.5 mol·L^{-1}) at 80 °C for 60 min for the elimination of LiCl and eventual impurities, followed by two washing steps in ultrapure water (Milli-Q/Millipore).

The acid doping process consisted of immersing the membranes in a 10 mol·L^{-1} phosphoric acid solution (*ortho*-H_3PO_4, Aldrich) for 5 days. The immersion time was defined after previous analysis of the weight change as a function of time; after this period elapsed, the membrane was removed from the acid, the surface was dried with filter paper, and the final weight was recorded.

2.2. Membrane Characterization. The acquisition of the water sorption ($\Delta m_{\%}$) and the doping sorption capacity ($\Delta m_{Dop\%}$) for undoped PBI and composite membranes was carried out by the same method using the ratio of the sorbed mass ($M_f - M_i$) and the mass of the pure and dry polymer (M_i), as described in eq 1.

$$\Delta m_{\%} = \frac{M_f - M_i}{M_i} \times 100 \quad (1)$$

The method for determining M_i consisted of dehydrating the membranes in a vacuum oven at 70 °C for 120 min and then measuring the dry mass. The measurement of M_f for water sorption was carried out by immersing the membranes in ultrapure water at room T for 3 h, drying their surface with a filter paper, and then immediate weighting until a constant mass was achieved. In addition, the M_f was estimated after immersing the membranes in H_3PO_4 (10 mol·L^{-1}) at room T for several days (up to 5 days). The ideal immersion time was evaluated by checking the weight gain until no further weight change was noticeable.

Acid doping level was estimated to obtain the number of acid molecules per monomeric unit of PBI; such index was calculated with the following equation:

$$\mathrm{ADL} = \frac{M_f - M_i}{M_i \times C_{\%PBI}} \times \frac{W_{PBI}}{W_{H_3PO_4}} \quad (2)$$

where $C_{\%PBI}$ stands for PBI concentration in the composite membrane concerning the mass of the added inorganic phase, and W_{PBI} and $W_{H_3PO_4}$ refer to the molar masses of both the repeating unit of PBI (308.34 for $C_{20}H_{12}N_4$) and the acid, respectively.

Thermogravimetric analysis (TGA) was performed in SETARAM equipment under N_2 flow (50 mL min^{-1}) from 25 to 900 °C at a heating rate of 10 °C·min^{-1}. The sample weight losses were measured in the undoped state so that the observed thermal events are mostly associated with water loss and polymer degradation.

The proton conductivity of the membranes was evaluated by impedance spectroscopy (IS) using the frequency response analyzer Solartron 1260. The measurements were conducted using an in-plane setup, conducting measurements using 4-probe terminals (Pt wires) in a commercial sample holder (FuelCon TrueXessory-PCM).[30,31] The IS measurements were carried out in the frequency range of 10^{-1}−10^6 Hz with an ac amplitude of 200 mV. Previous reports showed that in order to obtain reliable proton conductivity data from impedance spectra of ion-conducting polymers, the in-plane setup with 4 probes is indispensable to minimize nonlinear effects arising from electrode double-layer buildup across the electrodes.[31]

In order to obtain reliable results, the conductivity chamber was previously heated to 150 °C for 1 h to obtain a dried sample holder; afterward, the sample was inserted, and the conductivity chamber was reheated at 100 °C, from which the conductivity measurements were obtained stepwise in 10 up to 200 °C.

The morphology of PBI powder and the PBI membrane prepared by solution casting was evaluated by scanning electron microscopy SEM. The membranes were previously dried in a desiccator, followed by a sputtering deposition of gold. The equipment used was a JEOL instrument (JSM-6010LA).

2.3. Fuel Cell Tests. *2.3.1. Preparation of Membrane Electrode Assemblies.* The GDE consisted of two independent layers: a gas diffusion layer and a catalyst layer. The gas diffusion layer was based on carbon powder (Vulcan XC-72R, Cabot) with 15 wt % poly(tetrafluoroethylene) (PTFE, TE-306A, DuPont) deposited onto a carbon cloth substrate (Zoltek). Catalyst layers for single H_2/O_2 PEMFC were prepared by using Pt/C (40 wt %, Alfa Aesar) as the catalyst for both anode and cathode with a Pt loading of 1.0 mg cm^{-2}. For all samples, 30 wt % of powdered PBI or PBI film (cast from solution) was employed. The amount of PBI in the catalyst layer was estimated with respect to the mass of the electrocatalyst prior to acid doping.

The precursor catalytic ink was deposited onto the gas diffusion layer using spray coater equipment (PRISM-400 BT, USI - Ultrasonic Systems, Inc.). Two methods were employed to replace Nafion as the ionomeric phase in the catalytic layer (CL) of gas diffusion electrodes (GDE) for a high-temperature-resistant PBI: the conventional method for the catalytic ink preparation,[4−6] where a PBI/DMA solution is used to cast the PBI binder, which followed the same procedure for preparing the PBI membrane, and the alternative method that uses a powdered PBI in the catalytic ink. The conventional method consisted of an ink based on PBI/DMAc solution applied directly onto GDL. After ink deposition, the DMA solvent was evaporated (165 °C) and the electrodes were submitted to the same immersion in the H_3PO_4 doping process used for the membranes. The alternative method for powdered PBI consisted of drying the PBI powder in a vacuum oven at 70 °C for 1 h to eliminate excessive water and determine the dry weight. Next, the dry powder was immersed in a 10 mol·L^{-1} H_3PO_4 solution for 24 h under mechanical stirring at room temperature. The powder separation was carried out by vacuum filtration (0.22 μm filter), and the filtered PBI powder was washed with isopropanol to eliminate the acid excess. Then, the PBI powder was taken to a vacuum oven at 70 °C for 10 min to eliminate the isopropanol. As a sequence, the final weighing was carried out and the mass of absorbed acid by PBI powder was calculated (doping degree). The resulting H_3PO_4-doped PBI ionomer was added directly onto the gas diffusion layer (GDL) by spray

https://doi.org/10.1021/acsaem.4c01232
ACS Appl. Energy Mater. 2024, 7, 7759−7768

without an additional doping step. PBI is not an ionomer material and in order to avoid any technical jargon, the term "ionomer" is not employed to refer to the polymer electrolyte used in the catalyst layer, since it was traditionally misnamed after Nafion ionomer dispersions. The same applies to the term "binder" standing for PBI in the powder form since it may not act specifically as a binder and more as a support.

Different electrocatalysts were tested, namely, Pt/C (40% Pt, BASF), PtSn/C (3:1, 20% PtSn), and PtRu/C (1:1, 20% PtRu) with optimized membrane and GDE in HT-DEFC.

Membrane and electrode assemblies (MEAs) were fabricated by hot pressing the anode and the cathode to the H_3PO_4-doped PBI or PBI-SiO_2 membranes at 85 °C and 3 tons over 5 min.

2.3.2. HT-PEMFC and DEFC Tests. Initially, the fuel cells were optimized by using H_2 and O_2 gases to determine the ideal operating conditions for the different PBI materials. Both H_2 and O_2 were fed into the fuel cell without previous humidification. Fuel cell polarization measurements were carried out galvanostatically with a 5 cm^2 single cell (Electrocell, Brazil) with a serpentine flow pattern. Fuel cells were fed with dry gases, hydrogen (99.999%, White Martins), and oxygen (99.998, White Martins), at flow rates of 167 and 82 mL min^{-1}, respectively. The polarization curves were taken at different temperatures upon heating to 180 °C.

For HT-DEFC tests, H_2 was switched to an ethanol solution (5.7 mol·L^{-1}; 1:2 ethanol/water volume ratio) with a flux of 2 mL.min^{-1} using a Masterflex peristaltic pump (Cole-Parmer Instrument Company). Between the pump and the fuel cell, an in-house ethanol vaporizer made of stainless steel heated with a resistance heating strip was used to feed the ethanol. All of the fuel cell tests were conducted at 180 °C. A dc electronic load Agilent (6060B 3−60 V/0−60A) and a multimeter (U1252A) were used to monitor the fuel cell current and voltage.

3. RESULTS AND DISCUSSION

Figure 1 shows the water sorption (Figure 1a) and doping level (Figure 1b,c) for both undoped PBI and the PBI-SiO_2 composites as functions of the immersion time in phosphoric acid solution. Figure 1a shows that the water sorption capacity for undoped PBI and 2.5 wt % PBI-SiO_2 composite reaches equilibrium after a period of ∼5 h. Interestingly, both 5.0 and 10 wt % composites display an increasing sorption capacity up to the period in which the experiment was performed (22 h). As can be seen in Figure 1b, the stabilization of the doping weight change after immersion in H_3PO_4 is similar for the polymer and composites, indicating that at least 72 h is necessary for reaching the total PBI doping. Unexpectedly, the weight gains of doping observed for both PBI and PBI-SiO_2 composites for longer doping periods (t ∼ 120 h) are similar. Such feature is also evidenced by the different doping rates observed for t < 72 h, in which weight doping gain is more pronounced for composites than pure PBI, which is further evidence that the hydroxyl groups present at the SiO_2 surface contribute to the acid absorption. Such a result is relevant because it rules out performance variations of the composite due to the doping degree. Figure 1c shows that the degree of phosphoric acid doping slightly increases with the amount of added silica, in agreement with the data shown in Figure 1a.

Prior to the DEFC measurements, the configuration of gas diffusion electrodes was optimized by comparing GDE composed of PBI/DMA solution and PBI powder at the catalytic layer. Figure 2 shows representative SEM images displaying a comparison between electrodes prepared with a PBI/DMA solution (Figure 2a) and with a PBI powder (Figure 2b). Figure 2c shows the H_2/O_2 HT-PEMFC performances of both types of electrodes.

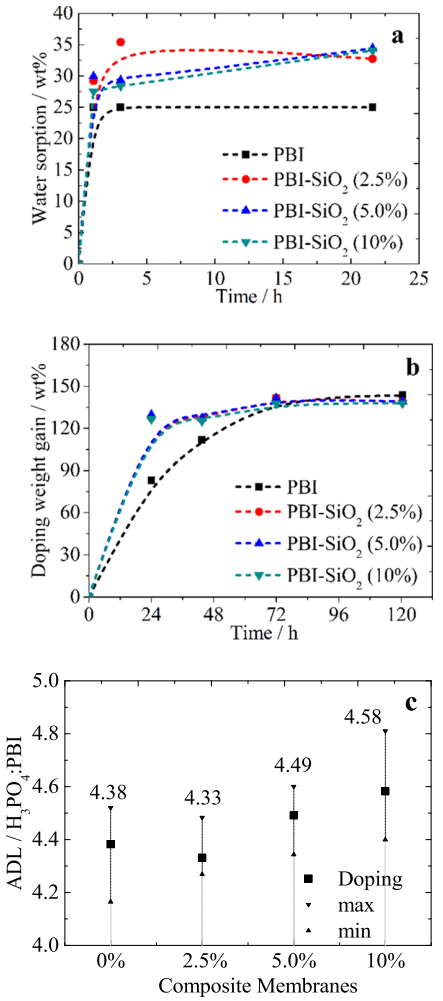

Figure 1. Water sorption (a); acid doping weight as a function of the immersion time in 10 mol·L^{-1} of H_3PO_4 (b); and the corresponding acid degree of doping (ADL) at 120 h (c) for undoped PBI and PBI-SiO_2 samples.

In the SEM images of Figure 2a,2b, the distinct morphologies of the PBI polymer as prepared from the PBI dissolved solution (Figure 2a) and the one prepared from the PBI powder dispersion (Figure 2b) are observed. The SEM measurements clearly evidence the compactness of PBI morphology as a film (prepared by a PBI solution) with respect to the PBI powder. Such a microstructural feature indicates that the morphology of the polymer modifies the percolation properties of the ionic conducting phase, resulting in a substantial enhancement of the fuel cell performance. Such an outcome is in accordance with previous findings.[32,33] In Figure 2c, it can be immediately noticed that the PEMFC can operate at high temperatures using acid-doped PBI at the catalytic layer in both film and powder forms. Possibly, the replacement of a fluorinated polymer for a nonperfluorinated one improved not only the thermal resistance of the polymer phase but also the interface by using the same material at both electrode and electrolyte phases. Figure 2c shows a remarkable improvement of the fuel cell performance, which is in accordance with previous reports that showed that the use of powdered ionic polymer increased the fuel cell performance as compared to the electrodes prepared with solubilized polymers.[27,28] It has been reported that the high concen-

https://doi.org/10.1021/acsaem.4c01232
ACS Appl. Energy Mater. 2024, 7, 7759−7768

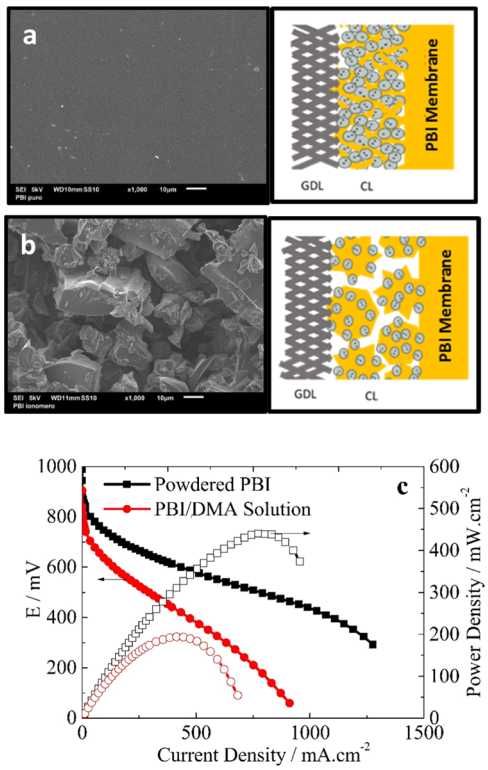

Figure 2. Scanning electron microscopy images of the PBI film prepared with the conventional method using PBI/DMA as a binder solution (a) and the PBI in powder form (b). The electrode microstructures are schematically represented by the alongside cartoons. (c) PEMFC electrochemical performances comparing both electrode materials at 180 °C.

trations of PBI binder in the catalytic inks prepared with solutions of PBI/DMA reduced the PEMFC performance due to a reduction of the catalytic layer porosity, and the PBI film can decrease the catalyst coverage by the fuel due to a reduction of the active sites and reduce the mass transport across the triple-phase boundary.[34,35] Moreover, below a critical value of 5 wt %, the lower concentrations of PBI powder resulted in lower performance, in this case, such effect was assigned to poor proton conduction due to an insufficient amount of the ion-conducting phase.[32] Another interesting feature observed in Figure 2c is related to the difference of $I-V$ slope at intermediate current densities. Since the electrolyte membrane is the same for both powder and film-like electrodes, the lower slope observed in the ohmic region is mostly associated with the proton conducting properties of the PBI used at the catalyst layer. The proton conductivities estimated from the linear $I-V$ slope for the PBI powder and film are $\sigma \sim 0.014$ and 0.007 S cm^{-1}, respectively. This result confirms a more extended proton conducting network existing in the electrode formed from powdered PBI.

It is worth noting that despite the irregular particle sizes and shapes displayed by PBI powder, no short-term fuel cell performance malfunction was observed due to any physical damage of the membrane. Possibly, PBI softening upon acid doping increases the electrode−electrolyte cohesion instead.

In order to evaluate the optimal PBI content at the catalyst layer on the fuel cell performance, HT-PEMFC H_2/O_2 polarization curves as a function of the PBI powder loading are shown in Figure S1. In Figure S1, it can be observed that the increase of the PBI loading from 2 to 20 wt % produced a marked increase in the fuel cell performance. The peak power density of HT-PEMFC using low PBI loading (2 wt %) is ∼300 mW cm^{-2}, which substantially increases when the amount of PBI is raised to 20 wt % (∼500 mW cm^{-2}). The further addition of PBI powder even at high concentrations of 40 wt % displayed no noticeable reduction in the fuel cell performance. Particularly, the 30 wt % PBI composition displayed higher current densities in the concentration polarization region, indicating that the mass transport is favored, and such composition was as such selected for the investigation of the performance of composite electrolyte membranes. It is worth mentioning that this high PBI powder loading is a unique feature compared with many electrocatalysts that are prepared in the traditional film-like form recommending a low PBI loading (<6 wt %) and opens up new pathways for composition optimization of catalytic layers for HT-PEMFC. The estimated Tafel coefficients for PBI/DMA solution (Figure S2), $b \sim 82$ mV dec^{-1}, are in accordance with previously reported data ($b \sim 80-120$ mV dec^{-1}).[24] However, the coefficients for the powdered PBI are significantly reduced ($b \sim 65$ mV dec^{-1}). The reduced Tafel coefficient for the powder PBI confirms that a higher catalytic activity is reached with the use of granulated PBI materials, which may be a result of the higher exposed platinum active sites for the redox reactions.

In this configuration, the porosity and ion conductivity of the catalytic layer play key roles in the fuel cell performance. The high-performance fuel cell in Figure 2c can be linked to both the impregnation of the carbon-supported catalyst into the polymer phase and to the percolation of the ion conduction into the acid-doped polymer electrolyte. The main morphological difference between the triple-phase boundary (TPB) prepared with PBI solution and PBI powder dispersion is that in the former, the carbon-supported catalyst is covered by a compact thin layer of acid-doped PBI film, while in the latter, the same carbon-supported catalyst is impregnated at the surface of the highly porous acid-doped powdered PBI. Possibly, the thin PBI layer covering the catalyst offers a conducting media for proton transport. On the other hand, the proton conduction in the catalytic layer formed with porous powdered PBI can take place via several pathways, such as the proton conduction in the catalyst-impregnated PBI powder, through the PBI bulk, or at the PBI powder surface and within the PBI particles in the H_3PO_4 phase, offering a lower resistance to the proton transport.

In addition to the new concept of "ionomeric" phase based on PBI powder, this study aimed to evaluate the effect of the addition of inorganic phase (SiO_2) incorporation into cast PBI membranes. The main goal of silica incorporation was to increase the HT-PEMFC and DEFC performance due to its inherent hygroscopic and reinforcement characteristics in organic−inorganic membranes.[36−39]

Thermogravimetric analysis was carried out for both undoped PBI and PBI-SiO_2 composites containing the highest amount of silica studied (10 wt %) aiming to evaluate the effect of nanoparticle incorporation in the PBI membranes on the thermal properties. Figure 3a shows the TGA runs for PBI and the PBI-SiO_2 (10 wt %) comparing the influence of the nanoparticles in the water retention and thermal stability of the composite samples. It can be observed that from RT up to 200 °C, the weight loss is dominated by the water evaporation from the samples, evidencing that the PBI-SiO_2 displayed a higher

https://doi.org/10.1021/acsaem.4c01232
ACS Appl. Energy Mater. 2024, 7, 7759−7768

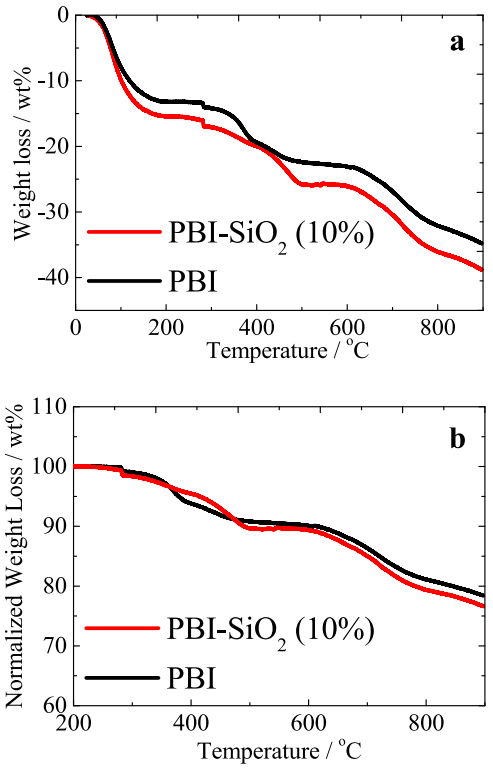

Figure 3. (a) TGA measurements for PBI and the PBI-SiO_2 (10 wt %) and (b) normalized TGA measurements with respect to the water content (b).

water sorption capacity than the pristine PBI membrane. This result is in good agreement with the water sorption capacity shown in Figure 1a.

The TGA runs in Figure 3b were compensated for with respect to water sorption. The TGA curves revealed a large weight loss (~10%) occurring from 400 up to 500 °C, for the polymer and the composite sample, respectively. The second weight loss observed is shifted to higher temperatures, as it can be observed that the onset of the weight loss is observed at 390 °C for PBI and ~500 °C for PBI-SiO_2. This feature has been previously observed for other silica-based PBI composite systems in which the inorganic particles delay the thermal degradation processes.[39] Further increasing the temperature shows a weight loss event taking place in the 600−800 °C range with a continuous weight loss above 800 °C. Both the polymer and composite samples exhibit similar weight losses at each event at $T > 200$ °C indicating negligible contribution to thermal degradation due to silica nanoparticles, which is an important aspect of the temperature dependence of proton conduction for such materials.

In order to identify the dc conductivity of acid-doped PBI membranes, impedance spectroscopy measurements were performed in the 4-probe configuration and are shown in Figure S3. The use of 4 probes widely spaced allows an improved estimation of the proton conductivity of the bulk of the samples. Moreover, by decoupling the potential and current sensing in the 4-probes configuration, the conductivity can be obtained exempt from electrode polarization influence.[31] Figure S3a shows that the impedance spectra of phosphoric acid-doped PBI without applied dc bias. PBI Nyquist plots have some features that resemble the spectra of Nafion membranes: (i) a nearly ideal high-frequency semicircle and (ii) a low-frequency semicircle.[31] The high-frequency semicircle can be fitted with an ideal parallel RC circuit (undepressed semicircle), and due to its high frequency (23 kHz), it can be attributed to an oscillatory motion of charges within short length scales that does not experience the long-range inhomogeneities of the polymeric structure.[31] Since this high-frequency arc represents a localized movement of charges, it does not represent the dc conductivity of the polymer, which is obtained from the total impedance of the sample—the sum of the high- and low-frequency resistances. The conductivities calculated from the high-frequency resistance (HFR) and the sum of the diameters of the HFR and LFR are $\sigma \sim 0.020$ and 0.013 S cm^{-1}, respectively. Since both conductivities resemble the ones estimated from the $I-V$ polarization curves (Figure 2c), which is a dc measurement, the HFR was erroneously assigned to the dc conductivity of the electrolyte membrane. In several representations and sample-holder configurations, the dc conductivity is observed at low frequencies ($f < 10^{-1}$ Hz),[9] in excellent agreement with Figure S3a. In Figure S3b, Nyquist plots of acid-doped PBI membranes are shown at different applied dc biases. The high-frequency semicircle is nearly independent of potential, whereas the low-frequency semicircle (Figure S3b) displays a strong dependence on the applied dc bias. Since in the 4-probe (in-plane setup) the electrode polarization is minimized, the observed potential-dependent behavior is possibly a result of Maxwell−Wagner−Sillars polarization across the polymeric microstructure[31]—the electric double layer formed within the polymer matrix arising from the buildup of charges across the polymer inhomogeneities—and represents a nonohmic contribution to the proton conductivity of PBI. This assignment is supported by the high dielectric constants observed for PBI found in the acid-doped state ($\Delta\varepsilon \sim 10^3-10^4$)[9,23] and by PBI X-ray patterns that indicate the existence of microstructural inhomogeneities in PBI.[9,23] This ionic polarization within the electrolyte membrane due to the double-layer charging was shown to represent an additional polarization loss in fuel cells, and since it is potential-dependent, it is inextricably mingled with the potential-dependent redox reactions. These recent findings have been bypassed in the proton conductivity studies of ionomers and of polymer imbibed with concentrated electrolytes.[40] Recently, the extreme difficulties encountered in isolating the contributions of each material component in an electrochemical system have been discussed.[41] How electrode and electrolyte processes are intrinsically inseparable is shown,[41] and the nonohmic behavior of the proton conductivity implies a revision of electrochemical analyses such as ohmic drop corrections in Tafel plots. Such a study comprises another communication and will be addressed in future work.

Figure 4 shows the temperature dependence of the proton conductivity, obtained from HFR, of both PBI and PBI-SiO_2 composite membranes (Figure 4a) and the corresponding Arrhenius plots (Figure 4b) (110−150 °C). In Figure 4a, the proton conductivity is in agreement with the reported values for the same temperature range (100−180 °C).[42]

In general, the addition of 2.5 wt % of silica improved the proton conductivity at an intermediate temperature range (ca. 100−190 °C). An interesting behavior is observed when the acid doping level (ADL) is compared with the proton conductivity data. The highest conductivity observed is for PBI-SiO_2 2.5 wt %, which compared to higher-inorganic-weight fractions absorbs the smallest amount of phosphoric

https://doi.org/10.1021/acsaem.4c01232
ACS Appl. Energy Mater. 2024, 7, 7759−7768

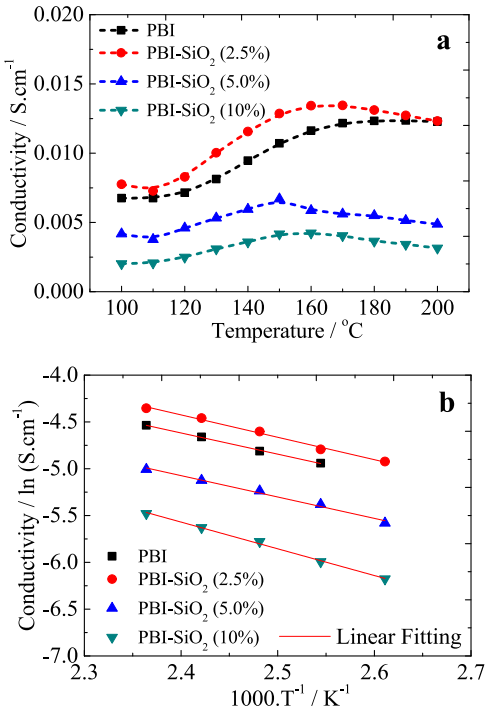

Figure 4. Proton conductivity dependence on temperature (a) and the corresponding Arrhenius plots (b) of PBI and PBI-SiO_2 composites.

acid (Figure 1c). The higher doping level achieved with increasing SiO_2 concentration promotes a reduction of the proton conductivity. The addition of silica (5 and 10 wt %) induces a drop of the conductivity values from ∼13.4 to ∼4.2 mS cm^{-1} (180 °C), which can be understood as an outcome of the lower mean free path for proton migration due to the insulating silica nanoparticles. All of the samples display a similar proton conductivity dependence on temperature. The proton conductivity exhibits a maximum in the 140−190 °C range. A maximum conductivity is observed for PBI polymer at ca. 180−190 °C, which decreases to ∼150 °C with increasing silica content in the PBI composites. According to the TGA data (Figure 3), there is no appreciable thermal degradation of the polymer chains up to ∼380 °C, and considering the glass transition temperature of PBI is at T_g ∼ 420 °C,[42] such thermal processes cannot account for the observed maximum in the conductivity in Figure 4a. Previous studies have demonstrated that PBI-like films exhibit at least three dielectric subrelaxation processes at temperatures below T_g.[9,23] The temperature dependence of the proton conductivity in PBI samples at T ∼ 100 °C can be influenced by such polymer relaxation, given that ionic conduction in amorphous materials is strongly linked to the motions of both main and side chains.[9,23,31,43] The temperature dependence of the proton conductivity can be related to the γ-relaxation occurring at T ∼ 225 °C.[9] This relaxation is attributed to local chain movements due to a rearrangement of the hydrogen-bonded network.[9] This feature helps understand the reduction of the maximum conductivity temperature of ∼40 °C for the PBI-SiO_2 composites. Since the γ-relaxation is associated with the state of the hydrogen-bonded network arrangement, the removal of water can result in an increment of the γ-relaxation time due to an improved chain packing.[9] The composite membranes display a higher water retention capacity, as evidenced in the water sorption measurements of Figure 1. This feature possibly improves the plasticization of the polymer chains, hence decreasing the temperature of the relaxation.

The calculated activation energy for the proton conduction of the composites from the Arrhenius plots of Figure 4b evidence that the addition of silica nanoparticles into PBI matrix increases the E_a in the following sequence: PBI (17.3 kJ mol^{-1}) < PBI-2.5 wt % SiO_2 (17.5 kJ mol^{-1}) < PBI-5.0 wt % SiO_2 (18.6 kJ mol^{-1}) < PBI-10 wt % SiO_2 (23.2 kJ mol^{-1}). The surface of silica nanoparticles is associated with a large variety of hydroxo-bridged complexes that can offer hydrogen-bonded structures with a broad range of interatomic distances and possibly affect the proton activation energy.

Figure 5 shows the H_2/O_2 fuel cell (PEMFC) performance using PBI-based composite membranes and powdered PBI electrodes.

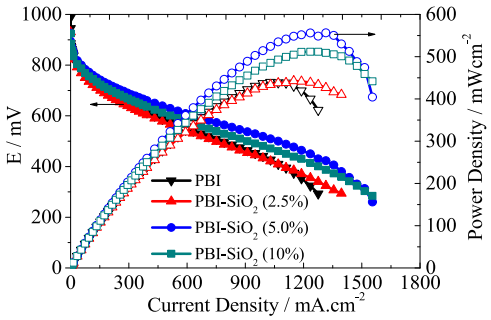

Figure 5. H_2-O_2 $I-V$ polarization curves for PBI and PBI composites with different weight fractions of the silica phase at 180 °C. Both anode and cathode were based on Pt/C (1.0 mg·cm^{-2}), PBI powder 30 wt %, and H_2 and O_2 flow rates of 167 and 82 mL·min^{-1}, respectively.

Figure 6 shows the performance of the same MEAs containing the composite membranes by replacing the hydrogen fuel for ethanol (DEFC) at 180 °C. In Figure 5, the electrochemical performance of the composite membranes with higher silica concentrations displayed higher power density values compared to pristine PBI. The PBI-SiO_2 containing 5 wt % of the inorganic phase displayed the highest power density, indicating that the performance of the hydrogen-fed fuel cell is a balance between the proton conductivity properties and the water retention properties. An improvement in the PEMFC peak power density from ∼438 mW cm^{-2} (PBI) to ∼557 mW cm^{-2} is observed for PBI-5 wt % SiO_2.

A similar trend is observed in Figure 6 for DEFC in which the PBI containing 10 wt % silica displayed the highest performance. The power density maxima for the composite membranes increase with increasing silica concentration: PBI (∼25 mW·cm^{-2}) < PBI-2.5 wt % SiO_2 (∼26 mW·cm^{-2}) < PBI-5.0 wt % SiO_2 (∼33 mW.cm^{-2}) < PBI-10 wt % SiO_2 (∼47 mW·cm^{-2}). Such unexpected relation between proton conductivity and the DEFC performance has already been observed for Nafion based composite membranes.[44] Compared to that of PEMFC (Figure 5), the performance of DEFC (Figure 6) is a trade-off between proton conduction and water retention, and the reduction of the ethanol crossover.[44] This finding reinforces that fuel cell efficiency is not only a result of the performance of each component separately, but interfacial features must be taken into account in order to better

https://doi.org/10.1021/acsaem.4c01232
ACS Appl. Energy Mater. 2024, 7, 7759−7768

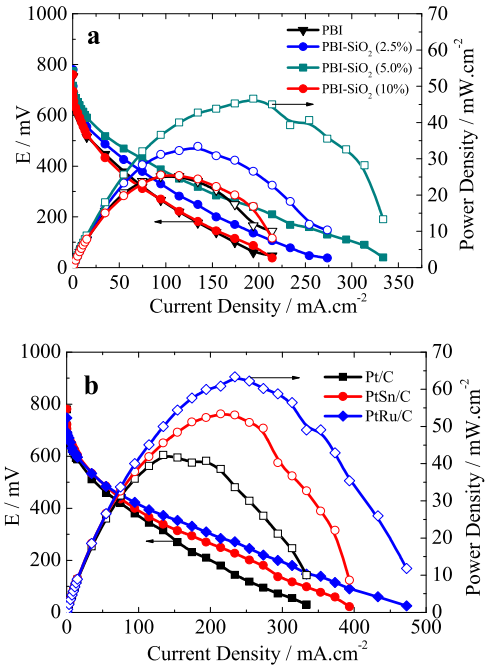

Figure 6. EtOH-O_2 $I-V$ polarization curves for PBI and PBI composites at T = 180 °C (a) and $I-V$ curves for 10 wt % PBI-SiO_2 using different types of anodic electrocatalysts: Pt/C (40%), PtRu/C (20%), and PtSn/C (20%) (b).

understand the main factors contributing to the overall fuel cell performance.

A marked increase of the open-circuit voltage (OCV) with increasing silica concentration from ∼753 mV (PBI) to ∼780 mV (5.0 wt % PBI-SiO_2) can be noted in Figure 6. The high operating temperature accelerates electrochemical reactions that contributed to the higher OCV compared to the low-temperature DEFC using Nafion both as a catalyst binder and as an electrolyte (∼400−600 mV).[37] Moreover, the addition of silica further increased the OCV values, mainly as a result of the suppression of the ethanol crossover from the anode to the cathode.

The DEFC performances using PBI membranes previously reported using PtRu (2 mg·cm^2)[45] and PtSn (4 mg·cm^2)[46] catalysts and operating at 200 °C showed peak power densities of 55.5 and 61.6 mW cm^{-2}, respectively. Thus, to improve the DEFC performance, the composite membrane with the optimum performance (10 wt % PBI-SiO_2) was selected to prepare MEAs with tailored electrocatalysts (Figure 6b). It can be observed that the DEFC power density can be significantly improved by alloying binary electrocatalysts more suitable for ethanol oxidation. The PtRu (1 mg·cm^{-2}) electrocatalyst sample reached higher values of power densities (∼64 mW cm^{-2}) than that of the platinum one (∼42 mW cm^{-2}), which corresponds to a performance increase of 65% enhancing both electrode and electrolyte components and, as a consequence, the electrode−electrolyte interface. Similarly, the Tafel coefficients estimated for the ethanol oxidation from Figure S4 for Pt, PtSn, and PtRu are b ∼ 128, 131, and 142 mV dec^{-1}, respectively. These values are in accordance with previously reported data[47] and evidence that the optimization performed for the H_2/O_2 fuel cells prevails when the fuel is replaced to ethanol. The active catalytic sites are exposed to the redox reactions for the PBI powder-impregnated electrocatalysts. Thus, by allying the multioperational parameters such as the triple-phase boundary morphology, the type of electrocatalyst employed, and the composite electrolyte, it was possible to effectively enhance the ethanol conversion to energy.

4. CONCLUSIONS

A significant enhancement of the high-temperature PEM fuel cell was achieved by the optimization of the electrochemical interfaces of both the electrode and the electrolyte. Such performance enhancement was possible by improving the electrode reactions and the electrolyte conductivity. Replacing the conventional binders at the catalyst layer by a powdered PBI significantly improved the triple-phase boundary allowing a 2-fold increase of the PEM fuel cell power density at 180 °C. This finding demonstrated that the PBI can be used in the electrodes at high temperatures eliminating the need of perfluorinated binders and allowing a relatively low metallic load of the electrocatalyst. The PEM fuel cell performance at high operating temperatures was further enhanced by PBI-SiO_2 composite electrolytes. Silica addition increased both the water retention capacity and the proton conductivity at higher temperatures while inhibiting the ethanol crossover. The combined properties of electrode−electrolyte interfaces resulted in an improvement in the performance of the direct ethanol fuel cell in the three characteristic polarization regions.

■ ASSOCIATED CONTENT

Supporting Information

The Supporting Information is available free of charge at https://pubs.acs.org/doi/10.1021/acsaem.4c01232.

H_2-O_2 $I-V$ polarization curves as a function of binder content; Tafel plots for H_2-O_2 $I-V$ polarization curves for powder and film-like PBI binder; potential dependence of impedance for acid-doped PBI at 200 °C at low frequencies; Tafel plots for ethanol; and $I-V$ polarization curves for PBI-SiO_2 using different electrocatalysts (PDF)

■ AUTHOR INFORMATION

Corresponding Author

Bruno Ribeiro de Matos − *Instituto de Pesquisas Energéticas e Nucleares (IPEN), 05008000 São Paulo, Brazil;* orcid.org/0000-0003-2022-6229; Email: brmatos@alumni.usp.br

Authors

Rodrigo Pires da Silva − *Instituto de Pesquisas Energéticas e Nucleares (IPEN), 05008000 São Paulo, Brazil*

Fabio Coral Fonseca − *Instituto de Pesquisas Energéticas e Nucleares (IPEN), 05008000 São Paulo, Brazil;* orcid.org/0000-0003-0708-2021

Elisabete Inacio Santiago − *Instituto de Pesquisas Energéticas e Nucleares (IPEN), 05008000 São Paulo, Brazil*

Complete contact information is available at: https://pubs.acs.org/10.1021/acsaem.4c01232

Funding

The Article Processing Charge for the publication of this research was funded by the Coordination for the Improvement of Higher Education Personnel - CAPES (ROR identifier: 00x0ma614).

Notes

The authors declare no competing financial interest.

■ ACKNOWLEDGMENTS

The authors are grateful for the support of the Brazilian National Council for Scientific and Technological Development CNPq Sis-H2 Grant No. 407967/2022-2, CNPq IBH2-MCTI Grant No. 405793/2022-7, and Fundação de Amparo à Pesquisa do Estado de São Paulo (FAPESP) Grant No. 2017/11937-4, 2022/07786-9. F.C.F. and E.I.S. are CNPq fellows.

■ REFERENCES

(1) *Climate Change 2023: Synthesis Report. Contribution of Working Groups I, II and III to the Sixth Assessment Report of the Intergovernmental Panel on Climate Change*; Lee, H.; Romero, J., Eds.; IPCC: Geneva, Switzerland, 2023; pp 35−115.

(2) İnci, M. Future vision of hydrogen fuel cells: A statistical review and research on applications, socio-economic impacts and forecasting prospects. *Sustainable Energy Technol. Assess.* **2022**, *53* (Part C), No. 102739.

(3) Berretti, E.; Osmieri, L.; Baglio, V.; Miller, H. A.; Filippi, J.; Vizza, F.; Santamaria, M.; Specchia, S.; Santoro, C.; Lavacchi, A. Direct Alcohol Fuel Cells: A Comparative Review of Acidic and Alkaline Systems. *Electrochem. Energy Rev.* **2023**, *6*, 30.

(4) Linares, J. J.; Sanches, C.; Paganin, V. A.; Gonzalez, E. R. Poly(2,5-bibenzimidazole) Membranes: Physico-Chemical Characterization Focused on Fuel Cell Applications. *J. Electrochem. Soc.* **2012**, *159*, F194−F202.

(5) Lobato, J.; Cañizares, P.; Rodrigo, M. A.; Linares, J. J.; López-Vizcaíno, R. Performance of a Vapor-Fed Polybenzimidazole (PBI)-Based Direct Methanol Fuel Cell. *Energy Fuels* **2008**, *22*, 3335.

(6) Zakaria, Z.; Kamarudin, S. K.; Timmiati, S. N. Membranes for direct ethanol fuel cells: An overview. *Appl. Energy* **2016**, *163*, 334.

(7) Li, Q.; He, R.; Jensen, J. O.; Bjerrum, N. J. PBI-Based Polymer Membranes for high temperature Fuel Cells − Preparation, Characterization and Fuel Cell Demonstration. *Fuel Cells* **2004**, *3*, 4.

(8) Quartarone, E.; Angioni, S.; Mustarelli, P. Polymer and Composite Membranes for Proton-Conducting, High-Temperature Fuel Cells: A Critical Review. *Materials* **2017**, *10*, 687.

(9) Nalawade, A.; Hassan, M. K.; Jarrett, W. A.; Mauritz, K. A.; Litt, M. H. Broadband dielectric spectroscopy studies of glassy-state relaxations in annealed poly(2,5-benzimidazole). *Polym. Int.* **2012**, *61*, 55.

(10) Rajabi, Z.; Javanbakht, M.; Hooshyari, K.; Badiei, A.; Adibi, M. High temperature composite membranes based on polybenzimidazole and dendrimer amine functionalized SBA-15 mesoporous silica for fuel cells. *New J. Chem.* **2020**, *44*, 5001.

(11) Li, X.; Ma, H.; Wang, P.; Liu, Z. C.; Peng, J. W.; Hu, W.; Jiang, Z. H.; Liu, B. J. Construction of High-Performance, High-Temperature Proton Exchange Membranes through Incorporating SiO_2 Nanoparticles into Novel Cross-linked Polybenzimidazole Networks. *ACS Appl. Mater. Interface* **2019**, *11*, 30735.

(12) Escorihuela, J.; Garcia-Bernabe, A.; Montero, A.; Andrio, A.; Sahuquillo, O.; Gimenez, E.; Compan, V. Proton Conductivity through Polybenzimidazole Composite Membranes Containing Silica Nanofiber Mats. *Polymers* **2019**, *11*, 182.

(13) Liu, L.; Li, H.; Chen, X.; Lei, X. Electrolyte Membranes Based on Molten $KH_5(PO_4)_{(2)}$ for Intermediate Temperature Fuel Cells. *Fuel Cells* **2019**, *19*, 280.

(14) Lee, S.; Seo, K.; Ghorpade, R. V.; Nam, K. H.; Han, H. High temperature anhydrous proton exchange membranes based on chemically-functionalized titanium/polybenzimidazole composites for fuel cells. *Mater. Lett.* **2020**, *263*, No. 127167.

(15) Ooi, Y. X.; Ya, K. Z.; Maegawa, K.; Tan, W. K.; Kawamura, G.; Muto, H.; Matsuda, A. Incorporation of titanium pyrophosphate in polybenzimidazole membrane for medium temperature dry PEFC application. *Solid State Ionics* **2020**, *344*, No. 115140.

(16) Ooi, Y. X.; Ya, K. Z.; Maegawa, K.; Tan, W. K.; Kawamura, G.; Muto, H.; Matsuda, A. CHS-WSiA doped hexafluoropropylidene-containing polybenzimidazole composite membranes for medium temperature dry fuel cells. *Int. J. Hydrogen Energy* **2019**, *44*, 32201.

(17) Ya, K. Z.; Nbelayim, P.; Tan, W. K.; Kawamura, G.; Muto, H.; Matsuda, A. Effects of cesium-substituted silicotungstic acid doped with polybenzimidazole membrane for the application of medium temperature polymer electrolyte fuel cells. *Int. Symp. Hydrogen Energy Energy Technol.* **2019**, *83*, 01008.

(18) Rao, S. S.; Hande, V. R.; Sawant, S. M.; Praveen, S.; Rath, S. K.; Sudarshan, K.; Ratna, D.; Patri, M. Alpha-ZrP Nanoreinforcement Overcomes the Trade-Off between Phosphoric Acid Dopability and Thermomechanical Properties: Nanocomposite HTPEM with Stable Fuel Cell Performance. *ACS Appl. Mater. Interfaces* **2019**, *11*, 37013.

(19) Kamaroddin, M. F. A.; Sabli, N.; Abdullah, T. A. T.; Abdullah, L. C.; Izhar, S.; Ripin, A.; Ahmad, A. Effect of Temperature and Current Density on Polybenzimidazole Zirconium Phosphate Hybrid Membrane in Copper Chloride Electrolysis for Hydrogen Production. *Int. J. Integr. Eng.* **2019**, *11*, 182.

(20) Cheng, Y.; Zhang, J.; Lu, S. F.; Jang, S. P. Significantly enhanced performance of direct methanol fuel cells at elevated temperatures. *J. Power Sources* **2020**, *450*, No. 227620.

(21) Bunno, T.; Maegawa, K.; Wlazło, M.; Hikima, K.; Nagai, A.; Matsuda, A. Ternary Triazole-Based Organic−Inorganic Proton-Conducting Hybrids Based on Computational Models for HT-PEMFC Application. *ACS Omega* **2023**, *8*, 44172−44182.

(22) Maegawa, K.; Ashida, Y.; Hikima, K.; Tan, W. K.; Kawamura, G.; Matsuda, A. Enhanced proton conductivity and power density of HT-PEMFCs using tin pyrophosphate microparticles-dispersed polybenzimidazole composite electrolyte membranes. *Solid State Ionics* **2023**, *393*, No. 116186.

(23) Saleha, W. F. G.; Ramesh, R.; Nalajala, N.; Ladewig, B. P.; Neerga, M. Dielectric relaxations in phosphoric acid-doped poly(2,5-benzimidazole) and its composite membranes. *J. Appl. Polym. Sci.* **2017**, *134*, No. 44867, DOI: 10.1002/app.44867.

(24) Park, J. O.; Kwon, K.; Cho, M. D.; Hong, S.-G.; Kim, T. Y.; Yoo, D. Y. Role of Binders in High Temperature PEMFC Electrode. *J. Electrochem. Soc.* **2011**, *158*, B675−B681.

(25) Arslan, F.; Dirsch, J.; Wagner, M.; Freiberg, A. T. S.; Komma, M.; Kerres, J.; Thiele, S.; Böhm, T. The influence of intrinsically proton conductive electrode binder materials on HT-PEMFC performance. *J. Power Sources* **2023**, *553*, No. 232297.

(26) Ahmed, Z.; Matos, B. R.; De Florio, D. Z.; Rey, J. F. Q.; Santiago, E. I.; Fonseca, F. C. Nafion-mesoporous silica composite electrolyte: properties and direct ethanol fuel cells performance. *Mater. Renewable Sustanable Energy* **2016**, *5*, 6.

(27) Poynton, S. D.; Slade, R. C. T.; Omasta, T. J.; Mustain, W. E.; Escudero-Cid, R.; Ocon, P.; Varcoe, J. R. Preparation of radiation-grafted powders for use as anion exchange ionomers in alkaline polymer electrolyte fuel cells. *J. Mater. Chem. A* **2014**, *2*, 5124.

(28) Biancolli, A. L. G.; Herranz, D.; Wang, L.; Stehlíková, G.; Bance-Soualhi, R.; Ponce-González, J.; Ocón, P.; Ticianelli, E. A.; Whelligan, D. K.; Varcoe, J. R.; Santiago, E. I. ETFE-based anion-exchange membrane ionomer powders for alkaline membrane fuel cells: a first performance comparison of head-group chemistry. *J. Mater. Chem. A* **2018**, *6*, 24330.

(29) Matos, B. R.; Santiago, E. I.; Rey, J. F. Q.; Fonseca, F. C. Origin of α and β relaxations of Nafion. *Phys. Rev. E* **2014**, *89*, No. 052601.

(30) Matos, B. R.; Andrade, C. A.; Santiago, E. I.; Muccillo, R.; Fonseca, F. C. Proton conductivity of perfluorosulfonate ionomers at high temperature and high relative humidity. *Appl. Phys. Lett.* **2014**, *104*, No. 091904.

(31) Matos, B. R. The genuine ac-to-dc proton conductivity crossover of nafion and polymer dielectric relaxations as a fuel cell polarization loss. *J. Electroanal. Chem.* **2020**, *871*, No. 114357.

(32) Parrondo, J.; Rao, C. V.; Ghatty, S. L.; Rambabu, B. Electrochemical Performance Measurements of PBI-Based High-Temperature PEMFCs. *Int. J. Electrochem.* **2011**, *2011*, No. 261065.

(33) Ohira, A.; Kuroda, S.; Mohamed, H. F. M.; Tavernier, B. Effect of interface on surface morphology and proton conduction of polymer electrolyte thin films. *Phys. Chem. Chem. Phys.* **2013**, *15*, 11494.

(34) Lobato, J.; Rodrigo, M. A.; Linares, J. J.; Scott, K. Effect of the catalytic ink preparation method on the performance of high

temperature polymer electrolyte membrane fuel cells. *J. Power Sources* **2006**, *157*, 284−292.
(35) Lobato, J.; Canizares, P.; Rodrigo, M. A.; Linares, J. J.; Pinar, F. J. Study of the influence of the amount of PBI−H3PO4 in the catalytic layer of a high temperature PEMFC. *Int. J. Hydrogen Energy* **2010**, *35*, 1347−1355.
(36) Panesi, A. R. Q.; Silva, R. P.; Cunha, E. F.; Korkischko, I.; Santiago, E. I. Three-dimensional CFD modeling of H_2/O_2 HT-PEMFC based on H_3PO_4-doped PBI membranes. *Ionics* **2021**, *27*, 3461−3475.
(37) Dresch, M. A.; Matos, B. R.; Godoi, D. R. M.; Linardi, M.; Fonseca, F. C.; Villullas, H. M.; Santiago, E. I. Advancing direct ethanol fuel cell operation at intermediate temperature by combining Nafion-hybrid electrolyte and well-alloyed PtSn/C electrocatalyst. *Int. J. Hydrogen Energy* **2021**, *46*, 13252−13264.
(38) Dresch, M. A.; Isidoro, R. A.; Linardi, M.; Rey, J. F. Q.; Fonseca, F. C.; Santiago, E. I. Influence of sol-gel media on the properties of Nafion-SiO_2 hybrid electrolytes for high performance proton exchange membrane fuel cells operating at high temperature and low humidity. *Electrochim. Acta* **2013**, *94*, 353−359.
(39) Deng, Q.; Wilkie, C. A.; Moore, R. B.; Mauritz, K. A. TGA−FTi.r. Investigation of the thermal degradation of Nafion and Nafion/[silicon oxide]-based nanocomposites. *Polymer* **1998**, *39*, 5961.
(40) Peng, J.; Wei, S.; Goenaga, G.; Weiss, C. M.; Neal, C. A.; Cantillo, N.; Zawodzinski, T. A. Investigate the equivalent weight effect on properties of perfluorosulfonic acid membrane in concentrated electrolytes. *Electrochim. Acta* **2022**, *431*, No. 141151.
(41) Huang, J.; Chen, Y.; Eikerling, M. Correlated surface-charging behaviors of two electrodes in an electrochemical cell. *Proc. Natl. Acad. Sci. U.S.A.* **2023**, *120*, No. e2307307120.
(42) Bouchet, R.; Siebert, E. Proton conduction in acid doped polybenzimidazole. *Solid State Ionics* **1999**, *118*, 287.
(43) da Silva, J. S.; Carvalho, S. G. M.; da Silva, R. P.; Tavares, A. C.; Schade, U.; Puskar, L.; Fonseca, F. C.; Matos, B. R. SAXS signature of the lamellar ordering of ionic domains of perfluorinated sulfonic-acid ionomers by electric and magnetic field-assisted casting. *Phys. Chem. Chem. Phys.* **2020**, *22*, 13764−13779.
(44) Matos, B. R.; Isidoro, R. A.; Santiago, E. I.; Fonseca, F. C. Performance enhancement of direct ethanol fuel cell using Nafion composites with high volume fraction of titania. *J. Power Sources* **2014**, *268*, 706.
(45) Linares, J. J.; Zignani, S. C.; Rocha, T. A.; Gonzalez, E. R. Ethanol oxidation on a high temperature PBI-based DEFC using Pt/C, PtRu/C and Pt3Sn/C as catalysts. *J. Appl. Electrochem.* **2013**, *43*, 147.
(46) Lobato, J.; Canizares, P.; Rodrigo, M. A.; Linares, J. J.; Sanchezrivera, B. In *Testing Different Catalysts for a Vapor-Fed PBI-Based Direct Ethanol Fuel Cell*, Proceedings of ASME 2009 Seventh International Fuel Cell Science, Engineering and Technology Conference, 2009.
(47) Zakaria, K.; McKay, M.; Thimmappa, R.; Hasan, M.; Mamlouk, M.; Scott, K. Direct Glycerol Fuel Cells: Comparison with Direct Methanol and Ethanol Fuel Cells. *ChemElectroChem* **2019**, *6*, 2578−2585.

NOTE ADDED AFTER ASAP PUBLICATION

Due to a production error, the version of this paper that was published ASAP September 2, 2024, had a tagging error in one of the author names. The corrected version was reposted September 6, 2024.

https://doi.org/10.1021/acsaem.4c01232
ACS Appl. Energy Mater. 2024, 7, 7759−7768